arXiv:2003.13184v2 [cond-mat.mes-hall] 25 Apr 2020

Wannier-type photonic higher-order topological corner states induced solely by gain and loss

Ya-Jie Wu,[1,2,*] Chao-Chen Liu,[1] and Junpeng Hou[2,†]

[1]*School of Science, Xi'an Technological University, Xi'an 710032, China*
[2]*Department of Physics, The University of Texas at Dallas, Richardson, Texas 75080-3021, USA*

Photonic crystals have provided a controllable platform to examine excitingly new topological states in open systems. In this work, we reveal photonic topological corner states in a photonic graphene with mirror-symmetrically patterned gain and loss. Such a nontrivial Wannier-type higher-order topological phase is achieved through solely tuning on-site gain/loss strengths, which leads to annihilation of the two valley Dirac cones at a time-reversal-symmetric point, as the gain and loss change the effective tunneling between adjacent sites. We find that the symmetry-protected photonic corner modes exhibit purely imaginary energies and the role of the Wannier center as the topological invariant is illustrated. For experimental considerations, we also examine the topological interface states near a domain wall. Our work introduces an interesting platform for non-Hermiticity-induced photonic higher-order topological insulators, which, with current experimental technologies, can be readily accessed.

I. INTRODUCTION

Topological phases and topological phase transitions in fermionic and bosonic systems, described by Hermitian Hamiltonians, have attracted great interest in the past three decades [1–3]. Recent studies have revealed that topological phases can be extended to non-Hermitian systems beyond the scope of closed systems [4–18]. Especially, the interplay between non-Hermiticity and topological states leads to unique properties that have no counterparts in Hermitian systems [19, 20]. While the non-Hermitian parameters are hard to tune in most classical or quantum systems, optical and photonic systems [21–27] provide controllable platforms to investigate non-Hermitian physics, in which the real and imaginary parts of the eigenenergy of a photonic mode are related to its frequency and amplifications/attenuations over time.

Photonic graphene, described by a two-dimensional (2D) honeycomb lattice consisting of optical cavities, exhibits various interesting features and thus has been intensively studied in past decades [3, 28–36]. It also enjoys significant advantages in terms of tunability of the lattice geometry and cleanness (absence of disorder or nonlinear interaction). Photonic graphene mimics a semimetal with two inequivalent gapless Dirac cones carrying opposite Berry phases $\pm\pi$. The local stability of Dirac points is guaranteed by time-reversal as well as inversion symmetries, while the global stability is protected by C_3 symmetry. By projecting Dirac points onto zigzag edges, the chiral surface states are raised, which have been observed in both electronic and photonic systems [37, 38]. In particular, the artificial photonic lattices provide an ideal platform for the simulation of non-equilibrium open systems with gain and loss. Photonic graphene with balanced gain and loss has been studied in previous work, and it is found that topologically protected edge states with non-degenerate purely imaginary energies appear along the zigzag edges [36].

More recently, a new type of topological phase, dubbed a higher-order topological state, was proposed [39–42]. Photonic systems provide a powerful experimental platform for higher-order topological insulators [43–46]. Formally, d-dimensional, r^{th}-order topological phases host $(d-r)$D topologically-protected edge states. For instance, a 2D/3D second-order topological insulator (SOTI) hosts zero-energy corner/hinge states while the $r=1$ cases reduce to the conventional topological insulators. The fate of higher-order topological corner states in open systems then becomes an important and intriguing question. Previous studies have employed either asymmetric intracell hopping [47, 48] or onsite gain/loss [49] to induce corner states based upon the 2D generalization of Su-Schrieffer-Heeger model on a square lattice [39].

In this paper, we enrich the family of non-Hermitian photonic SOTIs by proposing a minimal Wannier-type SOTI, solely induced by mirror-symmetric gain and loss, in photonic graphenes. We show that the photonic semimetal phase can be driven into a Wannier-type SOTI phase through tuning a stronger onsite gain/loss rate. Such a system hosts photonic corner modes and is characterized by a nontrivial topological invariant, known as the Wannier center or photonic polarization.

The paper is organized as follows. In Sec. II, we introduce a photonic graphene lattice with mirror-symmetric gain/loss and analyze relevant symmetries of the non-Hermitian Hamiltonian. In Sec. III, we study how the band structure changes with respect to increasing gain/loss strength and show there is a topological phase transition from a photonic semimetal to a photonic Wannier-type SOTI, characterized by a nontrivially quantized Wannier center [42, 50]. In Sec. IV, we examine the photonic higher-order topological corner states, and topological interface states at the domain wall of

*wuyajie@xatu.edu.cn
†junpeng.hou@utdallas.edu

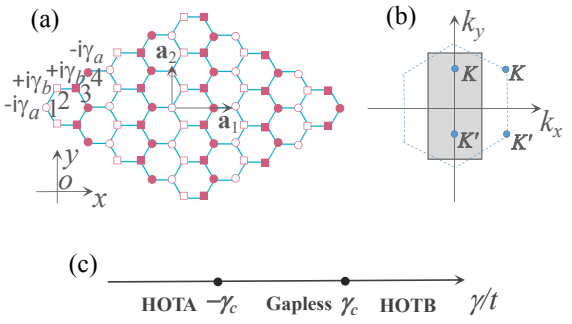


FIG. 1: (a) Illustration of photonic graphene lattice with patterned gain/loss $+i\gamma_b$ and $-i\gamma_a$. One unitcell consists of four sublattices indexed by 1 (circle), 2 (hollow square), 3 (solid square), and 4 (disk). (b) The dashed green curves sketch the first Brillouin zone of the original honeycomb lattice without gain and loss, while the gray shaded area indicates the first Brillouin zone corresponding to the enlarged unit cells of gain/loss-dressed lattice. (c) The phase diagram vs the strength of gain and loss γ in units of the bare nearest-neighbor hopping t.

two non-Hermitian photonic graphene. Finally, we make relevant discussions and draw conclusions in Sec. V.

II. PHOTONIC GRAPHENE WITH A PATTERNED GAIN AND LOSS

We consider uniformly coupled optical cavities on a honeycomb lattice, forming the photonic graphene. Each unitcell consists of four coupled resonators as shown in Fig. 1 (a). A mirror-symmetric imaginary onsite potential $(-i\gamma_a, i\gamma_b, i\gamma_b, -i\gamma_a)$ is introduced along x and we denote t as the bare coupling between nearest-neighbor cavities $\langle i_m, j_n\rangle$. The single-particle Hamiltonian is written as $H = H_0 + H_{\rm NH}$ and the Hermitian part reads $H_0 = -t\sum_{\langle i_m,j_n\rangle}\left(a^\dagger_{i_m}a_{j_n} + h.c.\right)$. The non-Hermitian potential is $H_{\rm NH} = -i\sum_{m,i}\gamma_m a^\dagger_{i_m}a_{i_m}$, where $\gamma_{m=1,4} = \gamma_a$ and $\gamma_{m=2,3} = -\gamma_b$ describe the patterned gain and loss. The operator $a^\dagger_{i_m}$ creates a photonic cavity mode at site i_m. Note that the non-Hermitian potential enlarges the unitcell of the usual honeycomb lattice, and the Bravais vectors are now given by $\mathbf{a}_1 = (3, 0)$ and $\mathbf{a}_2 = \left(0, \sqrt{3}\right)$, as illustrated in Fig. 1(a). The first Brillouin zone decreases correspondingly and it is sketched in Fig. 1(b). Here we set the lattice spacing of the graphene lattice to be a unit. The total Hamiltonian H in momentum space can be written as $H = \sum_k \Psi^\dagger_k H(k)\Psi_k$ in the basis $\Psi_k = (a_{1,k}, a_{3,k}, a_{2,k}, a_{4,k})^T$ and

$$\begin{aligned} H(k) &= \mathrm{Re}(\xi_k)\sigma_x\tau_0 - \mathrm{Im}(\xi_k)\sigma_y\tau_0 + \mathrm{Re}(\beta_k)\sigma_x\tau_x \\ &\quad - \mathrm{Im}(\beta_k)\sigma_y\tau_x - i\gamma_+\sigma_z\tau_z - i\gamma_-\sigma_0\tau_0, \end{aligned} \quad (1)$$

where $\mathrm{Re}(\xi_k) = -2t\cos\left(\sqrt{3}k_y/2\right)\cos(k_x/2)$, $\mathrm{Im}(\xi_k) = -2t\cos\left(\sqrt{3}k_y/2\right)\sin(k_x/2)$, $\mathrm{Re}(\beta_k) = -t\cos k_x$, $\mathrm{Im}(\beta_k) = -t\sin k_x$ and $\gamma_\pm = (\gamma_a \pm \gamma_b)/2$. The notations $\sigma_{x,y,z}$ and $\tau_{x,y,z}$ represent Pauli matrices while σ_0 and τ_0 are identity matrices.

In the absence of gain and loss ($\gamma_\pm = 0$), the Hamiltonian H describes the well-known graphene model with two stable Dirac points carrying geometric phases $\pm\pi$. The local stability of the Dirac points is protected by inversion symmetry ($\mathcal{P}$) and time-reversal symmetry ($\mathcal{T}$) while the global stability is guaranteed by C_3 rotational symmetry. In the presence of gain and loss, the C_3 symmetry is broken, but both $\mathcal{P}$ and $\mathcal{T}$ symmetries are respected when $\gamma_a = \gamma_b$. Hence, the system preserves $\mathcal{PT}$ symmetry as $(\mathcal{PT})H(k)(\mathcal{PT})^{-1} = H(k)$ with $\mathcal{PT} = \sigma_x\tau_0\mathcal{K}$, where $\mathcal{K}$ is complex-conjugation operator. In addition, there exist mirror symmetries along x and y, $\mathcal{M}_{x,y}H(k_{x,y})\mathcal{M}^{-1}_{x,y} = H(-k_{x,y})$ with $\mathcal{M}_x = \sigma_x\tau_x$ and $\mathcal{M}_y = \sigma_0\tau_0$, where the former is crucial for the topological characterization of the nontrivial HOTI phase.

Without loss of generality, we consider the special case $\gamma_a = \gamma_b = \gamma$, namely, $\gamma_- = 0$ and $\gamma_+ = \gamma$. The four bands in momentum space can be analytically solved as

$$\begin{aligned} E_{\pm,+}(k) &= \pm\sqrt{3t^2 + 2t^2\cos\left(\sqrt{3}k_y\right) - \gamma^2 + 2\sqrt{e_k}}, \\ E_{\pm,-}(k) &= \pm\sqrt{3t^2 + 2t^2\cos\left(\sqrt{3}k_y\right) - \gamma^2 - 2\sqrt{e_k}} \end{aligned} \quad (2)$$

where $e_k = 4t^4\cos^2\left(\sqrt{3}k_y/2\right)\cos^2(3k_x/2) - t^2\gamma^2$. Compared to the two bands in a usual graphene model, the energy bands here are folded and the Dirac points shift to $\mathbf{K}$ and $\mathbf{K}'$ due to the enlarged unit cell, as shown in Figs. 1(b) and 2(a_1). In the presence of gain and loss, there exist energy degeneracies $E_{+,+} = E_{+,-}$ and $E_{-,+} = E_{-,-}$ whenever $e_k = 0$. This corresponds to an exceptional ring in momentum space, which is given by $k_{\rm E} = 2\arccos\left[\gamma/\left(2t\cos(3k_x/2)\right)\right]/\sqrt{3}$ and is depicted in Figs. 2(b_2) and (c_2). For the eigenmodes inside the exceptional ring, we have $e_k > 0$ while $e_k < 0$ otherwise.

III. TOPOLOGICAL PHASE TRANSITIONS AND TOPOLOGICAL INVARIANTS

For each energy band $E_{\pm,\pm}(k)$, we could rewrite it as $E_{\pm,\pm}(k) = \mathrm{Re}\left[E_{\pm,\pm}(k)\right] + i\,\mathrm{Im}\left[E_{\pm,\pm}(k)\right]$. When the graphene lattice is free of gain and loss ($\gamma = 0$) , the energy bands are purely real and exhibit two Dirac points at $\mathbf{K} = \left(0, 2\sqrt{3}\pi/9\right)$ and $\mathbf{K}' = \left(0, -2\sqrt{3}\pi/9\right)$ [see Figs. 2(a_1) and (a_2)]. As γ increases, the exceptional ring gradually decreases, and the two Dirac points remain massless yet their locations in momentum space change. More explicitly, with larger γ, two Dirac points approach each other gradually [see Figs. 2(b_1) and (b_2)] and then merge at the time-reversal-invariant point $\Gamma = (0, 0)$ at critical gain/loss strength $\gamma_c = 1.732$ [see Figs. 2(c_1) and (c_2)]. Finally, when $\gamma > \gamma_c$ there opens a real energy gap, which is plotted in Figs. 2(d_1) and (d_2). Later, we will show

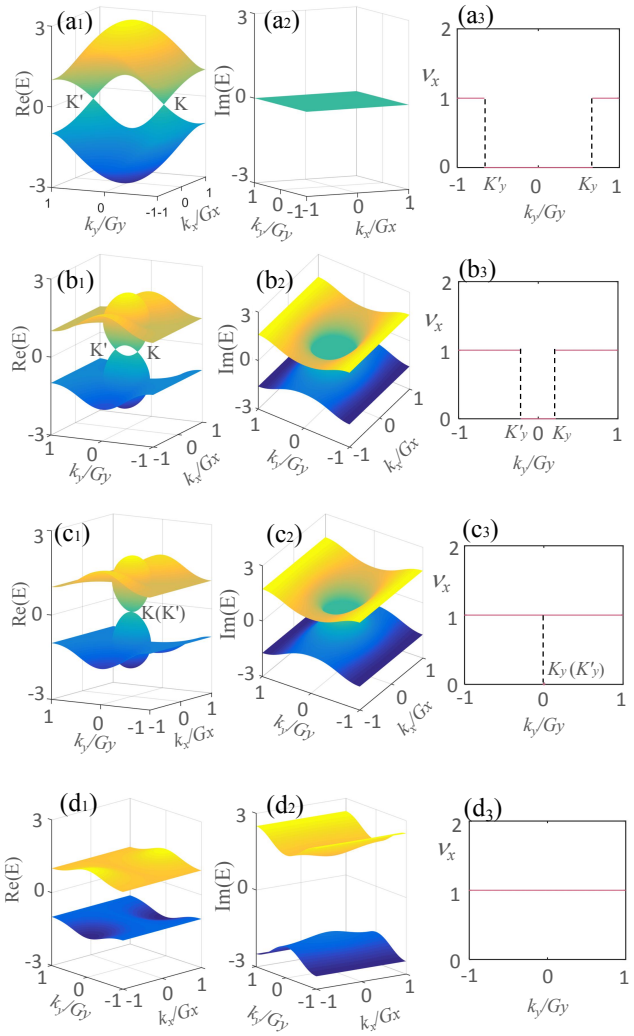


FIG. 2: Real spectrum (first column), imaginary spectrum (second column), and topological invariant (third column) at different gain/loss strengths. The non-Hermitian strength for each case is (a_1-a_3) $\gamma = 0$, (b_1-b_3) $\gamma = 1.6$, (c_1-c_3) $\gamma = 1.732$, and (d_1-d_3) $\gamma = 2.5$. Other parameters are chosen as $t = 1$, $G_x = \pi/3$, and $G_y = \pi/\sqrt{3}$.

that the phase transition described above has a topological nature.

Based upon the symmetry analyses in Sec. II, the Hamiltonian $H(k)$ preserves both $\mathcal{PT}$ symmetry and mirror symmetry along x. In particular, the reflection symmetry M_x leads to the nontrivial quantization of "photonic polarization" along the x direction. To formulate this as a bulk property, we construct a Wilson loop operator in x direction $W_{x,k}$, where k denotes the starting (base) point of the loop. We denote the Bloch wave function of the occupied energy bands with negative real energies as $\left|u^{R,L}_{m,k}\right\rangle$, where $\left|u^{L}_{m,k}\right\rangle$ and $\left|u^{R}_{m,k}\right\rangle$ are left and right eigenvectors defined as $H^{\dagger}(k)\left|u^{L}_{m,k}\right\rangle = E^{*}_{m}(k)\left|u^{L}_{m,k}\right\rangle$ and $H(k)\left|u^{R}_{m,k}\right\rangle = E_{m}(k)\left|u^{R}_{m,k}\right\rangle$ with normalization condition $\left\langle u^{L}_{m,k}|u^{R}_{n,k'}\right\rangle = \delta_{m,n}\delta_{k,k'}$. We define $[F_{x,k}]^{m,n} = \left(\left\langle u^{L}_{m,k+\Delta k_x}|u^{R}_{n,k}\right\rangle + \left\langle u^{R}_{m,k+\Delta k_x}|u^{L}_{n,k}\right\rangle\right)/2$, where $\Delta k_x = 2\pi/N_x$ with N_x the number of lattice sites along the x direction [51]. The Wilson loop operator is then $W_{x,k} = F_{x,k+N_x\Delta k_x}...F_{x,k+\Delta k_x}F_{x,k}$. We define the topological invariant $v_x(k_y) = -\frac{i}{\pi}\mathrm{Tr}\left(\ln W_{x,k}\right)$, forming the Wannier band. It is quantized under reflection symmetries. In the thermodynamic limit, the topological invariant at each k_y is

$$v_x(k_y) = -\frac{1}{\pi}\mathrm{Tr}\left(\oint \mathcal{A}_k dk_x\right), \tag{3}$$

where $(\mathcal{A}_k)_{m,n} = \left(\mathcal{A}^{LR}_k + \mathcal{A}^{RL}_k\right)/2$ is non-Abelian Berry connection with $\left(\mathcal{A}^{\alpha\beta}_k\right)_{mn} = -i\left\langle u^{\alpha}_{m,k}|\partial_{k_x}u^{\beta}_{n,k}\right\rangle$ and $\alpha,\beta = L,R$. Following similar steps, we could obtain the topological invariant $v_y(k_x)$ at each k_x. Finally, the topological invariant (Wannier center) of Wannier bands is defined as (v'_x, v'_y) with $v'_{x/y} = \frac{1}{4G_{y/x}}\oint v_{x/y}(k_{y/x})\,dk_{y/x}$, where $G_x = \pi/3$ and $G_y = \pi/\sqrt{3}$.

In the absence of gain and loss, topological invariants are $v_x(k_y) = 1$ if $-\pi/\sqrt{3} < k_y < -2\sqrt{3}\pi/9$ or $2\sqrt{3}\pi/9 < k_y < \pi/\sqrt{3}$ and $v_x(k_y) = 0$ otherwise [see Fig. 2(a_3)]. As the strength of gain and loss increases, we see the region with $v_x(k_y) = 1$ enlarges along k_y [see Fig. 2(b_3)]. At the critical point γ_c, $v_x(k_y) = 1$ at any k_y except the Dirac points $\mathbf{K}$ ($\mathbf{K}'$). Finally, when $\gamma > \gamma_c$, the real-energy gap opens, as shown in Fig. 2(d_1), with the topological invariant $v_x(k_y) = 1$ for all k_y. At this time, the Wannier center of the Wannier bands is quantized to a nontrivial value $(1/2, 0)$. Similar cases happen when $\gamma < 0$, and if $\gamma < -\gamma_c$, the Wannier center becomes $(-1/2, 0)$.

We would like to remark that the quantization of topological invariant v'_x is guaranteed by mirror symmetry along the x direction, and is robust against weak mirror-symmetric perturbations (see Appendix A for more details).

IV. WANNIER-TYPE TOPOLOGICAL CORNER MODES AND INTERFACE MODES

We focus on a sample shown in Fig. 1(a) and tune the parameters so that it is in topological phase with a Wannier center quantized to $(1/2, 0)$. We first consider the case $\gamma = 3.0$ and the numeric results are plotted in Fig. 3(a_1), where we observe two degenerate modes with purely imaginary energies. The corresponding particle density distributions are also plotted in Fig. 3(a_2), which shows that the two modes are localized at two horizonal corners of the given sample. We refer to this phase as second-order topological phase A (HOTA). Similarly, we find that the photonic topological corner modes also emerge when $\gamma < -\gamma_c$. This phase is dubbed second-order topological phase B (HOTB), and together with

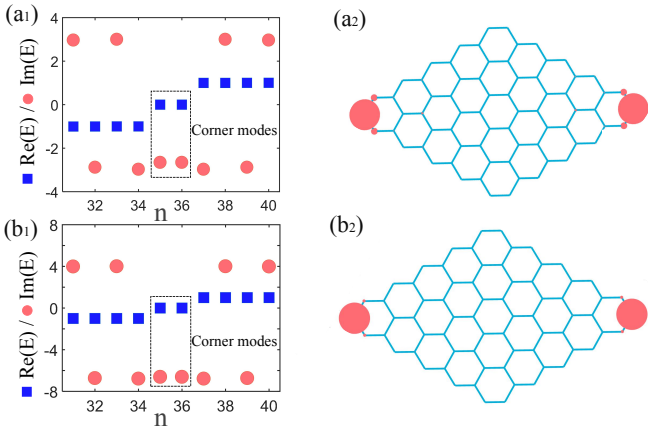


FIG. 3: (a_1) Real and imaginary parts of eigenspectrum [$\mathrm{Re}\,(E)$ and $\mathrm{Im}\,(E)$] vs the state index n. The two states in dashed rectangle are photonic corner modes with purely imaginary energies. (a_2) Spatial density distribution of the corner modes and the radii of the pink disk is proportional to local density. We choose $t = 1$ and $\gamma_a = \gamma_b = \gamma = 3$ in these two panels. (b_1, b_2) Similar to (a_1) and (a_2) but plotted with different gain/loss profiles $\gamma_a = 4.0$ and $\gamma_b = 6.8$, demonstrating the robustness of the photonic topological corner modes.

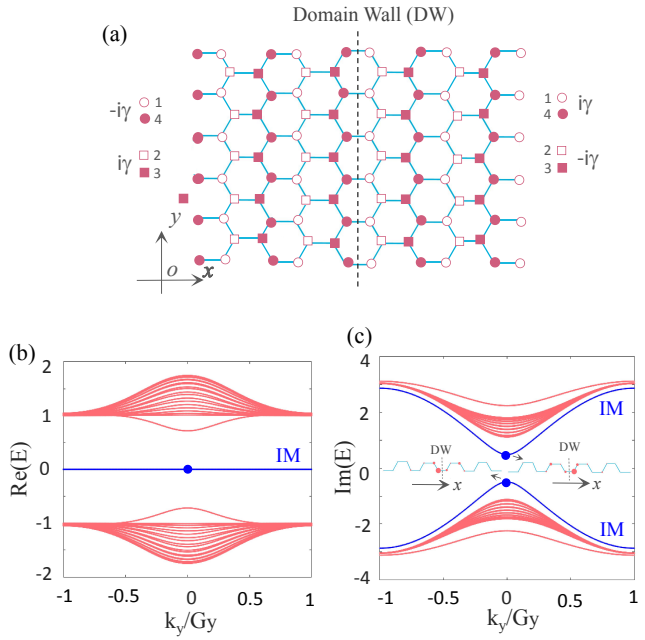


FIG. 4: (a) Two photonic graphene sheets with a domain wall (DW) in between, which is highlighted by the dashed line. As they possess opposite topological invariants, topological interface modes near the domain wall are raised. (b, c) Real and imaginary spectrum along k_y, with an open-boundary condition along x (total $N_x = 82$ sites), as specified in panel (a). The blue curve indicates the interface mode (IM). The insets depict the density distribution of two localized interface states. Parameters are set to be $t = 1$ and $\gamma_a = \gamma_b = \gamma = 3.2$.

HOTA they are illustrated in the phase diagram in Fig. 1(c). So far, we have focused on the special cases where $\gamma_a = \gamma_b$. However, from previous discussions, we have argued that the quantization of a nontrivial topological invariant is protected by the mirror symmetry, which is also preserved when $\gamma_a \neq \gamma_b$. Thus, we would expect the system to be nontrivial even when $\gamma_a \neq \gamma_b$, as long as the bulk spectrum is gapped. We demonstrate this point by showing the photonic corner modes in Figs. 3(b_1) and (b_2), where we set $\gamma_a = 4.0$ and $\gamma_b = 6.8$. This suggests that photonic corner modes are symmetry protected and they are robust against any mirror-symmetric perturbation. Here, we also would like to remark that our model also satisfies a pseudo-anti-Hermiticity, $H^\dagger(k) = -\eta H(k)\eta$, where $\eta = \sigma_z\tau_0$. This symmetry can lead to a nontrivial topology via chirality in terms of pairwise eigenvalues, E and $-E^*$. For a single corner state, it is also the eigenstate of the operator η. Therefore, the eigenenergy of the corner state satisfies $E = -E^*$, which suggests that the real component of energy of the corner state must be pinned at zero.

As discussed above, a photonic graphene with appropriate gain and loss γ is a photonic higher-order topological insulator characterized by topological invariant $(\mathrm{sign}(\gamma)/2, 0)$. In the following, we consider two photonic graphene sheets separated by a domain wall, which is depicted in Fig. 4(a). While the translation symmetry of graphene lattice is broken along x direction, the translation symmetry is respected along y. Hereafter, we consider k_y as a system parameter and treat $H(k_y)$ as one dimension. The system Hamiltonian then becomes

$$H = \sum_{i_x} H(i_x) = \sum_{i_x} H_0(i_x) + H_{\mathrm{NH}}(i_x), \qquad (4)$$

with

$$\begin{aligned} H_0(i_x) &= -t\sum\nolimits_{k_y} a^\dagger_{1,i_x,k_y} a_{4,i_x-1,k_y} + \xi_{k_y} a^\dagger_{1,i_x,k_y} a_{2,i_x,k_y} \\ &+ a^\dagger_{2,i_x,k_y} a_{3,i_x,k_y} + \xi^*_{k_y} a^\dagger_{3,i_x,k_y} a_{4,i_x,k_y} + H.C., \quad (5) \\ H_{\mathrm{NH}}(i_x) &= -i\sum_{m,k_y} \gamma_m \tilde{\eta}_m a^\dagger_{m,i_x,k_y} a_{m,i_x,k_y} \quad (6) \end{aligned}$$

where $\xi_{k_y} = t\left(1 + e^{i\sqrt{3}k_y}\right)$ and the domain wall structure is given by $\tilde{\eta}_{m=1,4} = -\tilde{\eta}_{m=2,3} = 1$ (left-hand side of the domina wall) and $\tilde{\eta}_{m=1,4} = -\tilde{\eta}_{m=2,3} = -1$ (right-hand side), as sketched in Fig. 4(a).

The energy spectra of the system are given by $H(i_x)|u(i_x,k_y)\rangle = E(k_y)|u(i_x,k_y)\rangle$. We set the strength of gain and loss so that both photonic graphene sheets are in the topological phases, where the left and right ones are HOTA and HOTB, respectively. Through numeric calculations, we find localized states with purely degenerate imaginary energy at the interface, i.e., the states with negative (positive) imaginary energy localize

at the left-hand (right-hand) side of the domain wall, as shown in Fig. 4(b) and (c). This confirms that the two topological phases (HOTA and HOTB) indeed exhibit different (in this case, opposite) topological properties and such a setup can be used for experimental study of photonic HOTI in photonic graphene.

In such a domain-wall structure, we may also consider the general imaginary potential $(-i\gamma_a, i\gamma_b, i\gamma_b, -i\gamma_a)$ with $\gamma_a \neq \gamma_b$ and the numeric calculations confirm the existence of topological localized interface modes. Finally, we also consider mirror-symmetric perturbations and find that, although the energies of bulk states vary, the photonic topological interface states with purely imaginary energy remain. In this sense, the topological interface states is symmetry protected.

V. DISCUSSION AND CONCLUSION

Mirror-symmetric onsite gain/loss brings about the real-energy gap in photonic graphenes and gives rise to localized photonic corner states with purely imaginary energy. Physically, this arises from the fact that the onsite imaginary potentials change the effective coupling between nearest-neighbor cavities, rendering an effectively anisotropic 2D photonic crystals. With increasing strength of gain and loss, the effective anisotropy of the photonic graphene grows. Correspondingly, the two Dirac cones (with opposite Berry phases) approach each other and annihilate at a high-symmetry point, leaving a gapped insulator phase, which tends out to be a photonic Wannier-type HOTI phase [42, 50].

Our proposal provides a realistic scheme to realize photonic topological corner states in photonic graphene. Moreover, it offers an accessible platform to study higher-order generalization of the topological insulator laser, which has been experimentally implemented in similar photonic crystal [52–55]. Topological corner modes show negative imaginary parts. They can be promoted to a lasing mode using high-Q cavities in visible or near-infrared range, and directly imaged in real space when properly excited [53].

We also remark that although the $\mathcal{PT}$ symmetry is respected in our system when $\gamma_a = \gamma_b$, our discussion here is irrelevant to the $\mathcal{PT}$-symmetric photonics studied in previous work [23]. In their setups, while $\mathcal{PT}$ is respected, both $\mathcal{P}$ and $\mathcal{T}$ are broken individually. Our gain/loss-dressed photonic graphene always preserves $\mathcal{P}$ (as well as $\mathcal{M}_x$) symmetry even when $\gamma_a \neq \gamma_b$ and it is known that spatial symmetry is crucial for stabilizing higher-order corner modes [40, 42]. In previous works, the topological properties of the $\mathcal{PT}$-symmetric systems usually originate from the Hermitian parts of Hamiltonians [56–59], but in our work non-Hermitian parts (patterned gain and loss) are crucial to induce the nontrivial phase. Moreover, current $\mathcal{PT}$-symmetric topological systems concern mainly 1D systems and the discussion of $\mathcal{PT}$ symmetry is limited to conventional topological phases [6, 22, 54, 59, 60], but our model presents a 2D higher-order counterpart.

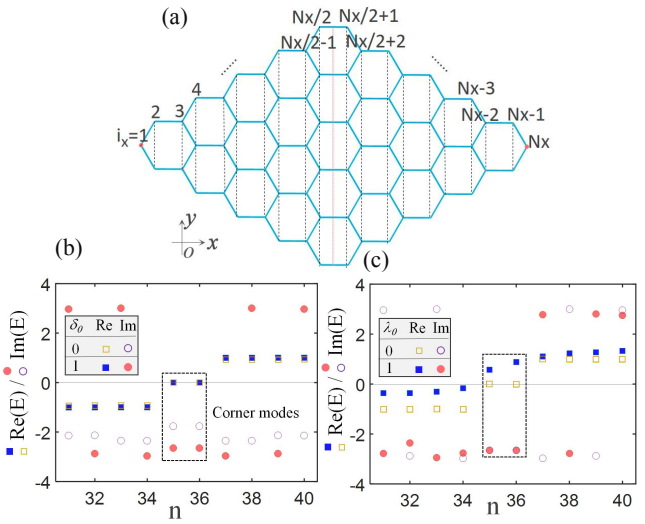


FIG. 5: (a) Illustration of honeycomb lattice with lattice index. The red dashed line indicates a mirror. (b) Real and imaginary parts of eigenenergies [$\mathrm{Re}\,(E)$ and $\mathrm{Im}\,(E)$] vs the state index n in the presence of random potentials (solid squares and dots). The hollow squares and circles represents the case without random potentials. The states in the dashed rectangle are photonic corner modes with purely imaginary energies. The amplitude of random potential $\delta_0 = 1$. (c) Similar to (b), but with a random potential that breaks reflection symmetry. The amplitude of random potential $\lambda_0 = 1$. Common parameters are $t = 1$, $\gamma = 3$.

In summary, we have revealed Wannier-type higher-order topological states in photonic graphenes with mirror-symmetric gain and loss. The symmetry-protected topological corner modes and interface modes are robust against perturbations respecting underlying symmetries. Our proposal does not require finely tuned spacing or cavity structures and thus, can be easily practiced in experiments.

Acknowledgments

This work is supported by the Scientific Research Program Funded by the Natural Science Basic Research Plan in the Shaanxi Province of China (Programs No. 2018JQ1058 and No. 2019JM-001), the NSFC under the Grant No. 11504285, the Scientific Research Program Funded by Shaanxi Provincial Education Department under the grant No. 18JK0397, and the Young Talent fund of the University Association for Science and Technology in Shaanxi, China (Program No. 20170608).

Appendix A: Robustness of corner states against perturbations

We consider two cases in the following to show the protection mechanism of higher-order topological states. First, we add general perturbation terms with the hypothesized reflection symmetry as $H_{pa} = i\sum_i \delta_i a_i^\dagger a_i$, where the potential $\delta_i = \delta_0 \kappa_{i_x}$, $\kappa_{i_x} = \kappa_{N_x - i_x + 1} \in [0, 1]$ is a random number for $i_x \leq N_x/2$, as shown in Fig. 5(a), and δ_0 is the amplitude of the random potential. Now the total Hamiltonian is $H_{\mathrm{T}} = H + H_{pa}$. Through numeric calculations, we find that localized corner modes with purely imaginary energies still remain, where only an imaginary energy shift appears for the topological corner states but the real component of their energy is pinned at zero, as sketched in Fig. 5(b). Therefore, the topological corner states are robust against random potentials (perturbations) with reflection symmetry.

Second, we add general random perturbation terms that break the hypothesized reflection symmetry as $H_{pb} = \sum_i \lambda_i a_i^\dagger a_i$, where $\lambda_i = \lambda_0 \kappa_i$, $\kappa_i \in [0, 1]$ is a random number. The numeric results are shown in Fig. 5(c). We find that the corner states acquire a non-zero real component of energy, and thus the corner states are no longer topologically protected.

To sum up, the corner states are robust against perturbations with reflection symmetry, but would disappear if the hypothesized reflection symmetry is broken by the random potential.

[1] M. Z. Hasan and C. L. Kane, Colloquium: Topological insulators, Rev. Mod. Phys. **82**, 3045 (2010).
[2] X.-L. Qi and S.-C. Zhang, Topological insulators and superconductors, Rev. Mod. Phys. **83**, 1057 (2011).
[3] T. Ozawa, H. M. Price, A. Amo, N. Goldman, M. Hafezi, L. Lu, M. C. Rechtsman, D. Schuster, J. Simon, O. Zilberberg, and I. Carusotto, Topological photonics, Rev. Mod. Phys. **91**, 015006 (2019).
[4] M. S. Rudner, and L. S. Levitov, Topological Transition in a Non-Hermitian Quantum Walk, Phys. Rev. Lett. **102**, 065703 (2009).
[5] A. Regensburger, M.-A. Miri, C. Bersch, J. Näger, G. Onishchukov, D. N. Christodoulides, and U. Peschel, Observation of Defect States in $\mathcal{PT}$-Symmetric Optical Lattices, Phys. Rev. Lett. **110**, 223902 (2013).
[6] T. E. Lee, Anomalous Edge State in a Non-Hermitian Lattice, Phys. Rev. Lett. **116**, 133903 (2016).
[7] D. Leykam, K. Y. Bliokh C. Huang, Y. D. Chong, and F. Nori, Edge Modes, Degeneracies, and Topological Numbers in Non-Hermitian Systems, Phys. Rev. Lett. **118**, 040401 (2017).
[8] Y. Xu, S.-T. Wang, and L.-M. Duan, Weyl Exceptional Rings in a Three-Dimensional Dissipative Cold Atomic Gas, Phys. Rev. Lett. **118**, 045701 (2017).
[9] L. Jin, Topological phases and edge states in a non-Hermitian trimerized optical lattice, Phys. Rev. A **96**, 032103 (2017).
[10] H. Shen, B. Zhen, and L. Fu, Topological Band Theory for Non-Hermitian Hamiltonians,Phys. Rev. Lett. **120**, 146402 (2018).
[11] F. K. Kunst, E. Edvardsson, J. C. Budich, and E. J. Bergholtz, Biorthogonal Bulk-Boundary Correspondence in Non-Hermitian Systems,Phys. Rev. Lett. **121**, 026808 (2018).
[12] S. Yao and Z. Wang, Edge States and Topological Invariants of Non-Hermitian Systems, Phys. Rev. Lett. **121**, 086803 (2018).
[13] S. Yao, F. Song, and Z. Wang, Non-Hermitian Chern Bands, Topological Phases of Non-Hermitian Systems, Phys. Rev. Lett. **121**, 136802 (2018).
[14] Z. Gong, Y. Ashida, K. Kawabata, K. Takasan, S. Higashikawa, and M. Ueda, Phys. Rev. X **8**, 031079 (2018).
[15] K. Yokomizo and S. Murakami, Non-Bloch Band Theory of Non-Hermitian Systems, Phys. Rev. Lett. **123**, 066404 (2019).
[16] Z. O. Turker and C. Yuce, Open and closed boundaries in non-Hermitian topological systems, Phys. Rev. A **99**, 022127 (2019).
[17] L. Jin and Z. Song, Bulk-boundary correspondence in a non-Hermitian system in one dimension with chiral inversion symmetry, Phys. Rev. B **99**, 081103(R) (2019).
[18] C.-H. Liu, H. Jiang, and S. Chen, Topological classification of non-Hermitian systems with reflection symmetry, Phys. Rev. B **99**, 125103 (2019).
[19] K. Kawabata, S. Higashikawa, Z. Gong, Y. Ashida, and M. Ueda, Topological unification of time-reversal and particle-hole symmetries in non-Hermitian physics, Nat. Commun. **10**, 297 (2019).
[20] S. Lieu, Topological symmetry classes for non-Hermitian models and connections to the bosonic Bogoliubov-de Gennes equation, Phys. Rev. B.**98**.115135 (2018).
[21] C. Poli, M. Bellec, U. Kuhl, F. Mortessagne, and H. Schomerus, Selective enhancement of topologically induced interface states in a dielectric resonator chain, Nat. Commun. **6**, 6710 (2015).
[22] A. Weimann, M. Kremer, Y. Plotnik, Y. Lumer, S. Nolte, K. Makris, M. Segev, M. Rechtsman, and A. Szameit, Topologically protected bound states in photonic parity time-symmetric crystals, Nat. Mater. **16**, 433 (2017).
[23] L. Feng, R. El-Ganainy, and L. Ge, Non-Hermitian photonics based on parity-time symmetry, Nat. Photonics **11**, 752 (2017).
[24] L. Xiao, X. Zhan, Z. H. Bian, K. K. Wang, X. Zhang, X. P. Wang, J. Li, K. Mochizuki, D. Kim, N. Kawakami, W. Yi, H. Obuse, B. C. Sanders, and P. Xue, Observation of topological edge states in parity-time-symmetric quantum walks, Nat. Phys. **13**, 1117 (2017).
[25] M.-A. Miri, A. Alù, Exceptional points in optics and photonics, Science **363**, eaar7709 (2019).
[26] P. St-Jean, V. Goblot, E. Galopin, A. Lemaître, T. Ozawa, L. L. Gratiet, I. Sagnes, J. Bloch, and A. Amo, Lasing in topological edge states of a one-dimensional lattice,Nat. Photonics **11**, 651 (2017).
[27] H. Zhao, P. Miao, M. H. Teimourpour, S. Malzard, R. El-Ganainy, H. Schomerus, and L. Feng, Topological hybrid silicon microlasers, Nat. Commun. **9**, 981 (2018).

[28] N. K. Efremidis, S. Sears, D. N. Christodoulides, J. W. Fleischer, and M. Segev, Discrete solitons in photorefractive optically induced photonic lattices, Phys. Rev. E **66**, 046602 (2002).

[29] G. Bartal, O. Cohen, H. Buljan, J. W. Fleischer, O. Manela, and M. Segev, Brillouin Zone Spectroscopy of Nonlinear Photonic Lattices, Phys. Rev. Lett. **94**, 163902 (2005).

[30] O. Peleg, G. Bartal, B. Freedman, O. Manela, M. Segev, and D. N. Christodoulides, Conical Diffraction and Gap Solitons in Honeycomb Photonic Lattices, Phys. Rev. Lett. **98**, 103901(2007).

[31] R. A. Sepkhanov, Y. B. Bazaliy, and C. W. J. Beenakker, Extremal transmission at the Dirac point of a photonic band structure, Phys. Rev. A **75**, 063813 (2007).

[32] O. Bahat-Treidel, O. Peleg, and M. Segev, Symmetry breaking in honeycomb photonic lattices, Opt. Lett. **33**, 2251 (2008).

[33] O. Bahat-Treidel, O. Peleg, M. Grobman, N. Shapira, M. Segev, and T. Pereg-Barnea, Klein Tunneling in Deformed Honeycomb Lattices, Phys. Rev. Lett. **104**, 063901 (2010).

[34] M. Polini, F. Guinea, M. Lewenstein, H. C. Manoharan, and V. Pellegrini, Artificial honeycomb lattices for electrons, atoms and photons, Nat. Nanotech. **8**, 625 (2013)

[35] Y. Plotnik, M. C. Rechtsman, D. Song, M. Heinrich, J. M. Zeuner, S. Nolte, Y. Lumer, N. Malkova, J. Xu, A. Szameit, Z. Chen and M. Segev, Observation of unconventional edge states in 'photonic graphene', Nat. Mater. **13**, 57 (2014).

[36] Z. Oztas and C. Yuce, Spontaneously broken particle-hole symmetry in photonic graphene with gain and loss, Phys. Rev. A **98,** 042104 (2018).

[37] Y. Kobayashi, K.-i. Fukui, T. Enoki, K. Kusakabe, and Y. Kaburagi, Observation of zigzag and armchair edges of graphite using scanning tunneling microscopy and spectroscopy, Phys. Rev. B **71**, 193406 (2005)

[38] M. C. Rechtsman, Y. Plotnik, J. M. Zeuner, D. Song, Z. Chen, A. Szameit, and M. Segev, Topological Creation and Destruction of Edge States in Photonic Graphene, Phys. Rev. Lett. **111**, 103901 (2013).

[39] W. A. Benalcazar, B. A. Bernevig, and T. L. Hughes, Quantized electric multipole insulators, Science **357**, 61(2017).

[40] J. Langbehn, Y. Peng, L. Trifunovic, F. von Oppen, and P. W. Brouwer, Refection-Symmetric Second-Order Topological Insulators and Superconductors, Phys. Rev. lett. **119**, 246401 (2017).

[41] Z. Song, Z. Fang, and C. Fang, $(d-2)$-Dimensional Edge States of Rotation Symmetry Protected Topological States, Phys. Rev. lett. **119**, 246402 (2017).

[42] M. Ezawa, Minimal models for Wannier-type higher-order topological insulators and phosphorene, Phys. Rev. B **98**, 045125 (2018).

[43] J. Noh, W. A. Benalcazar, S. Huang, M. J. Collins, K. P. Chen, T. L. Hughes, and M. C. Rechtsman, Topological protection of photonic mid-gap defect modes, Nat. Photonics **12**, 408(2018).

[44] X.-D. Chen, W.-M. Deng, F.-L. Shi, F.-L. Zhao, M. Chen, and J.-W. Dong, Direct Observation of Corner States in Second-Order Topological Photonic Crystal Slabs, Phys. Rev. Lett. **122**, 233902 (2019).

[45] A. E. Hassan, F. K. Kunst, A. Moritz, G. Andler, E. J. Bergholtz, and M. Bourennane, Corner states of light in photonic waveguides, Nat. Photonics **13**, 697 (2019).

[46] B.-Y. Xie, H.-F. Wang, H.-X. Wang, X.-Y. Zhu, J.-H. Jiang, M.-H. Lu, and Y.-F. Chen, Second-order photonic topological insulator with corner states, Phys. Rev. B **98**, 205147 (2018).

[47] T. Liu, Y.-R. Zhang, Q. Ai, Z. Gong, K. Kawabata, M. Ueda, and F. Nori, Second-Order Topological Phases in Non-Hermitian Systems, Phys. Rev. Lett. **122**, 076801(2019).

[48] C. H. Lee, L. Li, and J. Gong, Hybrid Higher-Order Skin-Topological Modes in Nonreciprocal Systems, Phys. Rev. Lett. **123**, 016805 (2019).

[49] X.-W. Luo and C. Zhang, Higher-Order Topological Corner States Induced by Gain and Loss, Phys. Rev. Lett. **123**, 073601 (2019).

[50] W. A. Benalcazar, T. Li, and T. L. Hughes, Quantization of fractional corner charge in C_n-symmetric higher-order topological crystalline insulators, Phys. Rev. B **99**,245151 (2019).

[51] J. Hou, Y.-J. Wu, and C. Zhang, Non-Hermitian topological phase transitions for quantum spin Hall insulators, arXiv: 1910.14606 (2019).

[52] G. Harari, M. A. Bandres, Y. Lumer, M. C. Rechtsman, Y. D. Chong, M. Khajavikhan, D. N. Christodoulides, and M. Segev, Topological insulator laser: Theory, Science **359**, eaar4003 (2018)

[53] M. A. Bandres, S. Wittek, G. Harari, M. Parto, J. Ren, M. Segev, D. N. Christodoulides, M. Khajavikhan, Topological insulator laser: Experiments, Science **359**, eaar4005 (2018)

[54] M. Parto, S. Wittek, H. Hodaei, G. Harari, M. A. Bandres, J. Ren, M. C. Rechtsman, M. Segev, D. N. Christodoulides, and M. Khajavikhan, Edge-Mode Lasing in 1D Topological Active Arrays, Phys. Rev. Lett. **120**, 113901 (2018).

[55] B. Bahari, A. Ndao, F. Vallini, A. E. Amili, Y. Fainman, and B. Kanté, Nonreciprocal lasing in topological cavities of arbitrary geometries, Science **358**, 636 (2017).

[56] F. K. Kunst, and V. Dwivedi, Non-Hermitian systems and topology: A transfer-matrix perspective, Phys. Rev. B **99**, 245116 (2019).

[57] J. M. Zeuner, M. C. Rechtsman, Y. Plotnik, Y. Lumer, S. Nolte, M. S. Rudner, Observation of a Topological Transition in the Bulk of a Non-Hermitian System, Phys. Rev. Lett. **115**, 040402 (2015).

[58] C. Yuce, Edge states at the interface of non-Hermitian systems, Phys. Rev. A **97**, 042118 (2018).

[59] R. Okugawa and T. Yokoyama, Topological exceptional surfaces in non-Hermitian systems with parity-time and parity-particle-hole symmetries, Phys. Rev. B **99**, 041202 (2019).

[60] K. Kawabata, Y. Ashida, H. Katsura, and M. Ueda, Parity-time-symmetric topological superconductor, Phys. Rev. B **98**, 085116 (2018).